Zhang *et al. Microstructures* 2023;3:2023046
DOI: 10.20517/microstructures.2023.57

Microstructures

Research Article

Open Access

Check for updates

Varied domain structures in $0.7Pb(Mg_{1/3}Nb_{2/3})O_3$ $-0.3PbTiO_3$ single crystals

Dawei Zhang[1,2,#], Lei Wang[1,#], Linglong Li[3], Pankaj Sharma[4,5], Jan Seidel[1,2]

[1]School of Materials Science and Engineering, UNSW Sydney, Sydney, NSW 2052, Australia.
[2]ARC Centre of Excellence in Future Low-Energy Electronics Technologies, UNSW Sydney, Sydney, NSW 2052, Australia.
[3]Key Laboratory of Quantum Materials and Devices of Ministry of Education, School of Physics, Southeast University, Nanjing 211189, Jiangsu, China.
[4]College of Science and Engineering, Flinders University, Bedford Park, Adelaide, SA 5042, Australia.
[5]Flinders Institute for Nanoscale Science and Technology, Flinders University, Adelaide, SA 5042, Australia.
[#]Authors contributed equally.

Correspondence to: Prof. Jan Seidel, School of Materials Science and Engineering, UNSW Sydney, Sydney, NSW 2052, Australia. E-mail: jan.seidel@unsw.edu.au

How to cite this article: Zhang D, Wang L, Li L, Sharma P, Seidel J. Varied domain structures in $0.7Pb(Mg_{1/3}Nb_{2/3})O_3$-$0.3PbTiO_3$ single crystals. *Microstructures* 2023;3:2023046. https://dx.doi.org/10.20517/microstructures.2023.57

Received: 13 Oct 2023 **First Decision:** 13 Nov 2023 **Revised:** 20 Nov 2023 **Accepted:** 28 Nov2023 **Published:** 1 Dec 2023

Academic Editor: Shujun Zhang **Copy Editor:** Fangyuan Liu **Production Editor:** Fangyuan Liu

Abstract

Single crystals of $0.7Pb(Mg_{1/3}Nb_{2/3})O_3$-$0.3PbTiO_3$ (PMN-30PT) with a composition close to the morphotropic phase boundary have demonstrated remarkable electromechanical properties, stimulating intensive research interest in the field of piezoelectrics. Domain structures have long been associated with their overall piezoelectric properties, thereby garnering particular research interest for the enhancement of piezoelectric properties. Here, we report on three distinct domain structures in this material. Through a combination of X-ray diffraction reciprocal space mapping and piezoresponse force microscopy measurements, an M_A crystal structure has been confirmed. The three-dimensional polar vectors of the three domain structures have been reconstructed with two $4M_A$ and one $2M_A$ domain structures. Correlations between different domain structures and their local electrical switching properties have been revealed. Our study of the PMN-30PT single crystal examines diverse domain structures at the mesoscale in detail, which provides valuable insight into the relationship between structures and properties of the material.

Keywords: Ferroelectrics, PMN-PT single crystal, domain structures, piezoresponse force microscopy

INTRODUCTION

Relaxor ferroelectric solid solutions of (1-x)Pb($Mg_{1/3}Nb_{2/3}$)O_3-$x$$PbTiO_3$ (PMN-xPT) have long been the research focus over the last few decades by virtue of their superb piezoelectric and electromechanical performance that is closely related to their complex microstructure[1-6]. In pursuit of high piezoelectric properties, normally two approaches are adopted: the intrinsic one through composition tuning of the solid solution or doping[5,7,8] and the extrinsic one through domain/domain wall engineering[9-11]. To achieve high electromechanical properties in the PMN-xPT system, regarding the intrinsic approach, the composition x is usually tuned to a composition of x~0.3 near the morphotropic phase boundary (MPB), which separates the rhombohedral and tetragonal phases. The improved piezoelectric performance has been attributed to the intermediate monoclinic phase bridging the adjacent rhombohedral and tetragonal phases, thus allowing easy polarization rotation[2,8,12]. The resulting domain structures at the MPB region in various systems have also demonstrated beyond-binary multilevel switching and memristive behavior, which is promising for the new paradigms of non-volatile memory applications[13,14]. When it comes to the extrinsic approach, both direct current (DC) poling and an emerging alternating current (AC) poling approach, along with various other approaches, have been utilized to enhance the piezoelectricity through domain wall engineering[1,3,15-28].

Therefore, PMN-30PT is of particular research interest for revealing its structure-property relationship. This interest stems not only from its status as an MPB composition but also from its rich domain structures. From the composition perspective, the hierarchy of domain structures has been known to evolve with different Ti concentrations. Pb($Mg_{1/3}Nb_{2/3}$)O_3 (PMN) and $PbTiO_3$ (PT) are typical relaxors and classic ferroelectric systems featuring short-range-ordered polar nanoregions and long-range-ordered domains, respectively. The increased concentration of PT leads to an increased off-center polar displacement within the unit cell accompanied by mechanical stress[29,30]. To accommodate the elastic strain, smaller domains are self-assembled into larger ones with orientations along the polarization variants. Bian *et al.* have investigated the domain structures of PMN-xPT systems at diverse compositions and their associated local piezoresponse[31]. From the domain engineering perspective, significant effort has been made to examine the relationship between the domain structure and the electromechanical performance in PMN-xPT systems. The piezoelectric response of PMN-PT has been enhanced more than three times by increasing the domain wall density through DC poling[1,16]. Recently, it has been found that three varied domain structures can be induced by the DC poling on the patterned electrodes[32]. Under AC poling, it is suggested that the field-induced M_A phase contributes to the enhanced piezoelectricity in PMN-PT[22]. It has also been discovered that with increasing AC poling cycles, the domain structure can evolve from 4R to 2R with a concomitant increasing length of 109° domain walls[23]. To note, 4R/2R denotes that there are four/two possible spontaneous polarization directions along the polar axis in the rhombohedral phase[23]. Additionally, the elimination of light-scattering 71° domain walls has been used to fabricate transparent PMN-PT single crystals under AC poling[3,33].

In this work, three distinctive domain structures have been revealed in different regions of PMN-30PT single crystals using piezoresponse force microscopy (PFM). X-ray diffraction (XRD) reciprocal space mappings (RSM), a series of rotational in-plane (IP) PFM, and trailing field experiments have been used to confirm the M_A structure of the crystal, and three-dimensional (3D) polar domain variants have been reconstructed. The correlation between the domain structures and the local electrical switching properties has been revealed using switching spectroscopy PFM (SSPFM).

EXPERIMENTAL METHODS

PMN-30PT single crystals with (100) orientation were obtained from MTI Corporation, China. The crystals were synthesized by an improved Bridgman method. The size of the crystals is 5 mm × 5 mm × 0.2 mm, two-sided polished with a surface roughness (Ra) less than 10 Å.

High-resolution θ-2θ XRD studies and RSMs were carried out using a PANalytical X'Pert Pro diffractometer with $CuK_{\alpha-1}$ radiation. The optical images were taken using a Nikon ECLIPSE LV100POL optical microscope.

All measurements were performed by two commercial AFM systems, an AIST-NT Smart scanning probe microscopy (SPM) 1000 and an Asylum Research MFP-3D Infinity at room temperature under ambient conditions. The IP PFM signal depends on the sample orientation with respect to the cantilever. It means that only the projected component of the IP polarization vector perpendicular to the cantilever contributes to the IP PFM signal, as IP PFM modes rely on the torsional vibration of the cantilever. Therefore, in order to resolve the IP polarization vectors, angle-resolved PFM measurements were carried out by changing the azimuthal angle between the cantilever and the sample. Consequently, the directions of the IP polarization variants have been resolved by high-resolution PFM images acquired at the quasi-identical region by changing the cantilever-sample orientation from 0° to 360° with an interval of 45°. To note, during the angle-resolved PFM measurements, the orientation of the cantilever is fixed, and only the angle of the sample is rotated with respect to the cantilever. The angle-resolved PFM measurements were performed with an AC excitation bias between 1.0 to 2.0 V (peak to peak) with platinum-coated tips (HQ:NSC35/Pt, Mikromasch) at an off-resonance frequency of 100 kHz to avoid any crosstalk from the topography or resonance frequencies. For SSPFM measurements, commercial silicon tips with conductive Ti/Ir coating (ASYELEC.01-R2, Asylum Research) were used.

RESULTS AND DISCUSSION

The composition of PMN-30PT single crystals is at the MPB that separates the rhombohedral and tetragonal phases, and the existence of intermediate monoclinic phases at this regime is argued to facilitate the rotation path between these two phases. To analyze the polarization variants in the sample, RSMs were performed to determine the crystal structure. A twofold and a threefold peak splitting were observed around 310 and 311 reflections, respectively, confirming a monoclinic A (M_A) structure [Supplementary Figure 1][34,35].

Type 1 domain structures with a typical zigzag feature on the topography are shown in Figure 1. The long vertical zigzag stripes [Figure 1A], with an average stripe/domain width of 2.5 mm, can be observed in the majority of the sample regions, as evidenced by the optical image shown in Figure 1G. Coinciding with the topography, the out-of-plane (OOP) phase shows the same zigzag domain structure, with a clear 180° phase reversal between the adjacent two stripe domains [Figure 1B]. Such topography-domain correlation originates from a mechanochemical polishing effect that leads to a polarization-dependent mechanical property upon polishing. Of note, the downward polarization demonstrates a higher surface height in comparison to the upward polarization, as confirmed in the OOP poling experiment in Supplementary Figure 2. Two sets of IP PFM images [Figure 1C-F] were obtained by changing the tip-sample rotation angle from 0 to 90 to resolve the IP polarization variants as the polarization component perpendicular to the cantilever leads to a torsional movement of the cantilever that can be sensitively detected. The 0° and 90° rotation IP PFM phase signals in Figure 1C and E show checkerboard domain structures with four-color contrast, indicating four polarization variants. Figure 1C and E is then binarized to Figure 1D and F with only black and white contrast. The trailing field, which is equivalent to an IP

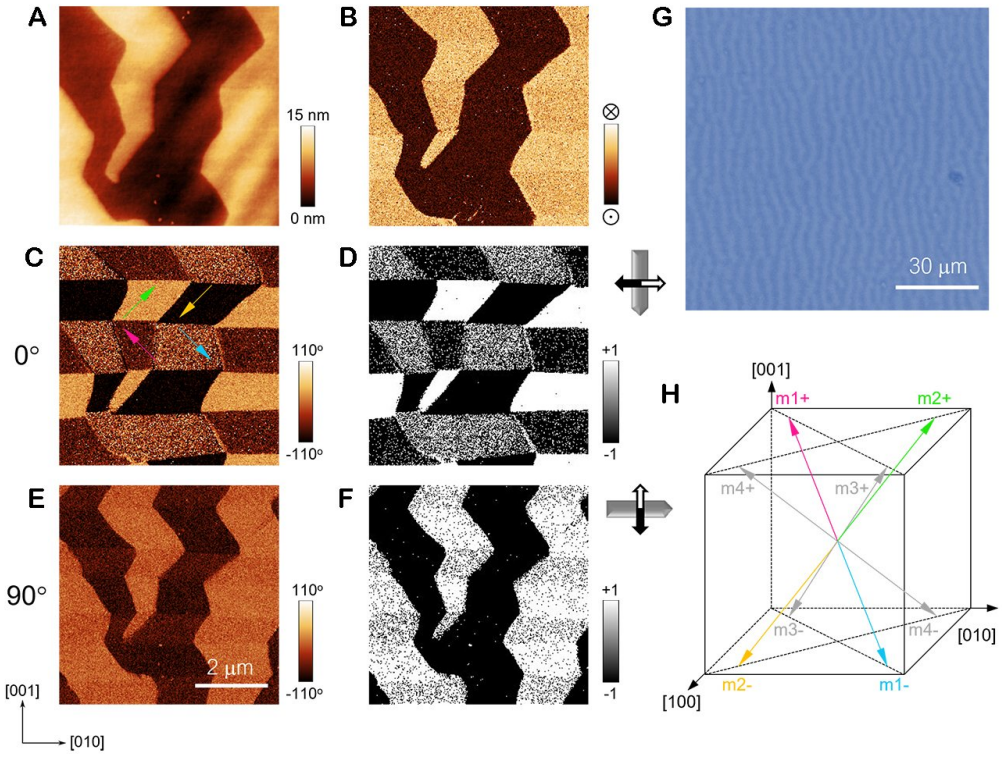

Figure 1. Type 1 domain structure. (A) Topography of type 1 domain structure. (B) The corresponding OOP phase signal. (C) IP phase signal measured at a tip-sample orientation of 0. The IP polarization variants are denoted on each domain. (D) The binarized version of (C). (E) IP phase signal measured at a tip-sample orientation of 90. (F) The binarized version of (E). (G) The optical image of type 1 domain. (H) The reconstructed three-dimensional polarization vectors for type 1 domain.

electric field with a direction co-determined by the tip motion direction and the polarity of the tip bias, has been used to resolve the directions of the binary black and white contrast [Supplementary Figure 3][36]. All the PFM signals in this paper were measured at off-resonance frequency to avoid the crosstalk from the topography and possible phase flipping near the resonance frequency. By combining the two IP directions, as denoted in Figure 1D and F, the polarization vectors for each domain can be established in this (100) oriented M_A PMN-PT sample. The IP projections of the four variants are shown in Figure 1C. Additionally, in Supplementary Figure 4, full angle-resolved PFM measurements were performed at the quasi-identical region by altering the cantilever-sample orientation from 0° to 360° at an interval of 45°. IP phase values of the four domains are plotted as a function of tip rotation angle, and then trigonometric fitting is used to resolve the relative phase differences between each of the four domains. The same reconstruction result of the polarization vectors is obtained and shown in Supplementary Figure 5, which is also confirmed by the trailing field experiments shown in Supplementary Figures 6 and 7. The domain structure shows a $4M_A$ domain configuration with non-charged head-to-tail 71° domain walls (m1+ and m2+, m1- and m2-) and 180° domain walls (m2+ and m2-, m1+ and m1-), which can be seen from the reconstructed four polarization vectors shown in Figure 1H. There are no 109° domain walls in this type 1 domain structure. To note, the PMN-30PT is an MPB composition with an M_A structure, which closely resembles the rhombohedral structure due to the slight structural deviations; therefore, the names of domain wall types still conform to the conventional usage, denoted as 71, 109, and 180, as defined within a pseudocubic structure[37,38].

Type 2 domain structures with a checkerboard feature in the topography are shown in Figure 2. The alternating yellow and brown quadrilateral patterns [Figure 2A], with an average base/height of 1.5/3 mm, can only be observed in a minority of the sample regions embedded in the matrix of type 1 domain configurations. The OOP phase image shows the same alternating checkerboard domains in comparison with the topography, exhibiting distinct 180° phase differences [Figure 2B]. The optical image shows a consistent checkerboard pattern [Figure 2G]. Two sets of IP PFM images with different tip-sample orientations, i.e., 0° and 90°, were measured to determine the polarization vectors [Figure 2C and E]. Based on the binarized IP phase values [Figure 2D and F], the reconstructed four polarization vectors with both upward and downward directions are shown in the schematic in Figure 2H. The IP polarization projections are denoted in corresponding domains in Figure 2C. Compared to the type I domain structure, 71° domains are non-existent, but 109° domain walls emerge (m1+ and m3+, m1- and m3-) in addition to the 180° domain walls that are present in both type 1 and type 2 domain structures. The existence of 180° domain walls in both type 1 and 2 domain structures is due to the allowed polarization states in both upward and downward directions.

Type 3 domain structures have a prominent horizontal long stripe domain arrangement along [010], as shown in Figure 3A. The stripes have a typical width of around 1-2 mm. Not all stripe domains are continuous, as some of them terminate or merge to form larger stripes. The OOP phase also demonstrates a clear 180° phase difference between adjacent stripe domains, as shown in Figure 3B. The optical image also shows a consistent structure, as shown in Figure 3C. It should be noted that the type 3 domain only emerges at certain regions that are adjacent to the sample edge, as denoted by the red dashed boxes in Supplementary Figure 8. The same rotational experiments were done and are shown in Figure 3D-G. The 0° rotational IP phase signals [Figure 3D and E] show the same phase contrast as the OOP phase signal [Figure 3B]. The 90° rotational IP phase signals [Figure 3F and G], by contrast, present a uniform bright phase contrast. This indicates that the polarization components perpendicular to the cantilever from all variants now have the same direction with respect to the cantilever. The reconstructed polarization vectors with only two allowed directions, sharing the same m1+ and m3+ variants as compared to the type 2 domain, are shown in the schematic in Figure 3H. In this domain configuration, only non-charged 109° domain walls exist due to the existence of only two polarization variants.

A PMN-xPT system is a well-known relaxor ferroelectric system, and the hierarchy of domain structures is known to vary on length scales from nanometer to millimeter with different Ti concentrations. PMN is a pure relaxor with short-range-ordered polar nano regions (PNRs), while PT is a classical ferroelectric with long-range-ordered large domain structures. The introduction of Ti^{4+} increases the off-center displacement, and the distortion inside the PNRs results in a mechanical mismatch between regions with different polarization orientations. To accommodate the generated mechanical strain or minimize the elastic energy, the small PNRs tend to amalgamate into larger domains of micrometer sizes, such as the observed stripe domains or checkboard patterns, following their macroscopic symmetries[31]. The observed domain configurations in all three types of domains show macroscopic domain structures, which is consistent with previous studies[3,21,31,32]. On a close inspection, type 1 and 2 domain structures, while both showing a clear four-variant domain configuration, are slightly different from the commonly reported ones[3,21,32]. A very typical four-rhombohedral domain configuration after DC or AC poling will have four allowed polarization orientations only in the OOP directions[3,21], either upward or downward. A checkerboard domain structure along [110] directions and alternating long stripe domains along [010] directions are presented for the OOP and IP domain structures, respectively. The coexistence of 71° and 109° domains and the absence of 180° domains are seen. By comparison, a type 1 domain shows zigzag and checkboard domain structures in the OOP and IP images, respectively, with a coexistence of 71° and 180° domains. Type 2 does show a

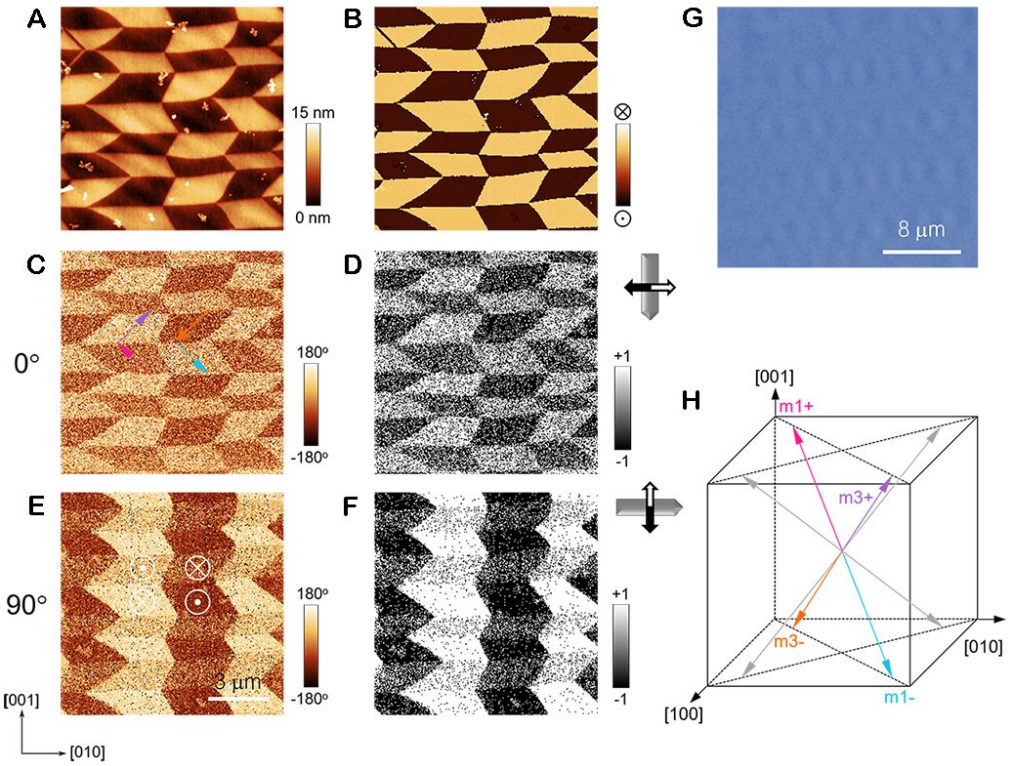

Figure 2. Type 2 domain structure. (A) Topography of type 2 domain structure. (B) The corresponding OOP phase signal. (C) IP phase signal measured at a tip-sample orientation of 0. The IP polarization variants are denoted on each domain. (D) The binarized version of (C). (E) IP phase signal measured at a tip-sample orientation of 90. (F) The binarized version of (E). (G) The optical image of type 2 domain. (H) The reconstructed three-dimensional polarization vectors for type 2 domain.

checkerboard domain structure in the OOP plane but no alternating stripe domains, with a coexistence of 109° and 180° domains. A Type 3 domain structure is consistent with the reported 2M configuration, showing long stripe domains in both OOP and IP directions. One unique feature of the type 3 domain is the existence of pure 109 domain walls that do not induce light scattering in comparison to 71 domain walls, making transparent crystals possible[3]. However, due to the small fraction of the type 3 domain, the transparency of the region is not very apparent under the optical microscope [Supplementary Figure 8]. The formation of a type 3 domain structure may be due to the unusual strain state at the edge of the dented region [Supplementary Figure 8]. It is known that strain can effectively modify the domain structures or even alter the phase in the PMN-PT system[39,40], which is especially prominent in the PMN-30PT system, which is close to the MPB and, therefore, has a small anisotropy.

The local ferroelectric properties are further probed by SSPFM mappings of the three different types of domains [Figure 4]. The imprint field mappings calculated from the SSPFM mapping ($V_i = (|V_p| - |V_n|)/2$), where V_p and V_n are positive and negative switching voltages, are also shown. The typical topography image for type I domain structures with OOP polarization directions is shown in Figure 4A. The corresponding V_i mapping exhibits a nice correlation with the topographical feature, which also resembles the domain structure in the OOP direction, as shown in Figure 4A. Figure 4C shows the SSPFM curve averaged over 200 groups of data (100 groups of data each for downward and upward domains). Figure 4D-I contain the same information on the topography, the V_i imprint mapping, and the averaged SSPFM curve for type II and type III domain structures, respectively. The extracted critical fields for each domain type have been summarized in Table 1. $V_{i\text{-SSPFM}}$ and $V_{i\text{-map}}$ are the imprint fields extracted from the averaged SSPFM curve

Table 1. Local switching properties of the three types of domain structures

Type	$V_{i\text{-}SSPFM}$ (V)	$V_{i\text{-}map}$ (V)	$V_{c\text{-}SSPFM}$ (V)	$V_{c\text{-}map}$ (V)
Type 1	-0.6	-1.28	7.1	7
Type 2	-3.55	-3.5	13.77	14
Type 3	-0.95	1.5	11.9	11.5

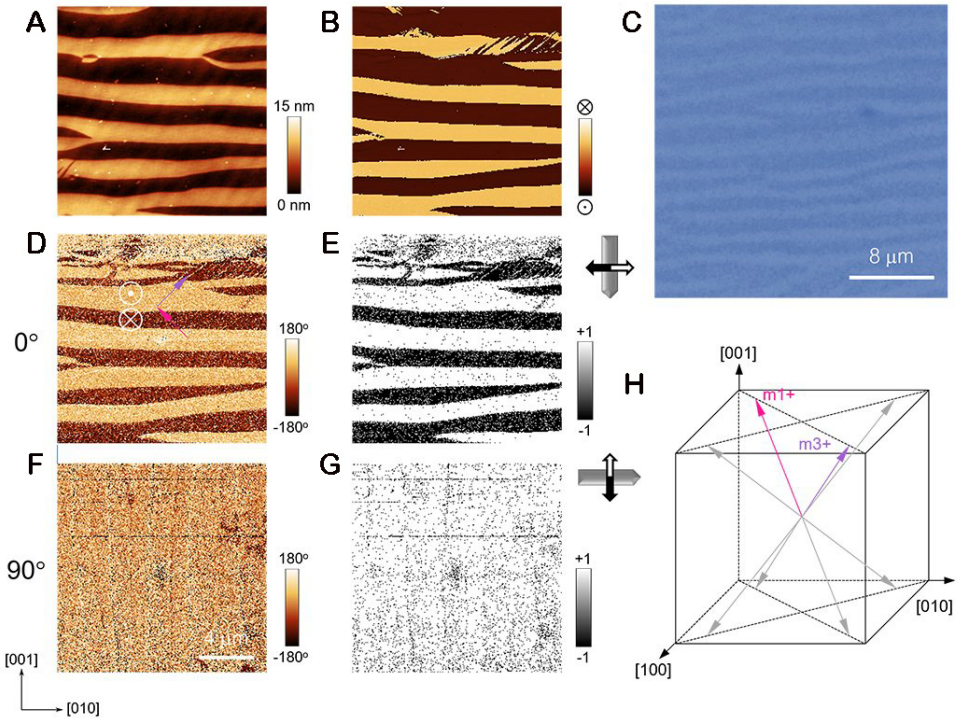

Figure 3. Type 3 domain structure. (A) Topography of type 3 domain structure. (B) The corresponding OOP phase signal. (C) The optical image of type 3 domain. (D) IP phase signal measured at a tip-sample orientation of 0. The IP polarization variants are denoted on each domain. (E) The binarized version of (D). (F) IP phase signal measured at a tip-sample orientation of 90. (G) The binarized version of (F). (H) The reconstructed three-dimensional polarization vectors for type 3 domain.

and the SSPFM mappings, respectively. $V_{c\text{-}SSPFM}$ and $V_{c\text{-}map}$ are coercive fields extracted from the averaged SSPFM curve and the SSPFM mappings, respectively, where $V_c = (|V_p| + |V_n|)/2$. From the imprint mappings [Figure 4B, E, H], it can be seen that in all three types of domain structures, the downward domains consistently have a negative imprint while the upward domains have a positive imprint, which may be due to the alignment of the high concentration of defect dipoles, e.g., oxygen vacancies, during the DC switching processes. $V_{i\text{-}map}$ for type 1, 2, and 3 domain structures are -1.28, -3.5, and 1.5 V, respectively. As a comparison, $V_{i\text{-}SSPFM}$ shows a similar trend (-0.6, -3.55, and -0.95 V), and the deviation might originate from different sample sizes as the $V_{i\text{-}SSPFM}$ is based on only 200 groups of datasets. The coercive fields, $V_{c\text{-}SSPFM}$ and $V_{c\text{-}map}$, show that a type I domain structure has the smallest coercive field, around 7 V, compared to about 14 and 11 V for type 2 and 3 domain structures. The divergence is probably due to the different polarization variants in type 1, m1 and m2, in contrast to m1 and m3 in type 2 and 3 domain structures. The resultant vectors m1+ and m2+ or m1- and m2- are closer to the OOP direction of the electric field along the [100] directions than m1 and m3 pairs, which allows the electrical switching at a lower voltage. The coercive field of the type 3 domain is slightly smaller than that of the type 2 domain. It is possible that a larger domain size

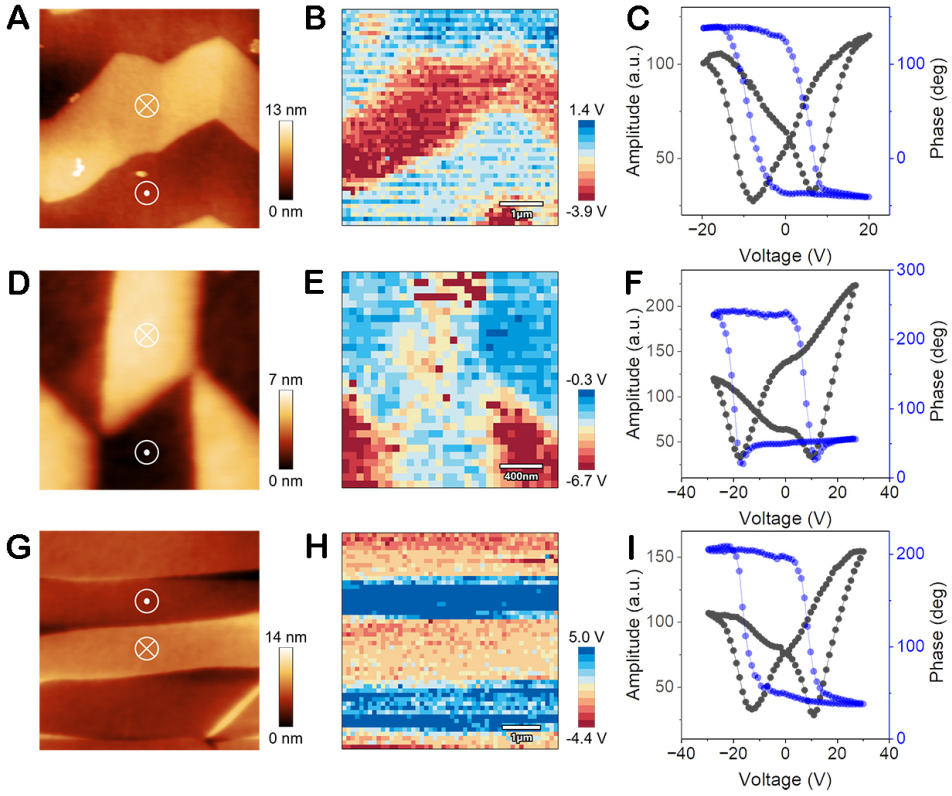

Figure 4. Local electrical switching properties for three types of domains. (A-C) The topography, SSPFM mapping, and averaged SSPFM curves for type 1 domain. (D-F) The topography, SSPFM mapping, and averaged SSPFM curves for type 2 domain. (G-I) The topography, SSPFM mapping, and averaged SSPFM curves for type 3 domain.

in the type 3 domain leads to a larger depolarization field and elastic energy, which makes the domain unstable and easier to switch. The detailed $V_{c\text{-}map}$ mappings and averaged SSPFM loops for upward and downward domains are shown in Supplementary Figure 9. The cross-boundary regions between type 1 and type 3, alongside those type 1 and type 2, are shown by the optical microscope images in Supplementary Figure 10.

CONCLUSION

In summary, three different types of domain structures have been systematically studied using SPM in PMN-30 PT single crystals with an M_A crystal structure. High-resolution PFM and trailing field experiments were performed to reconstruct the polarization variants in 3D space for three different domain structures. Type 1 and 2 domain structures have been shown to possess two varying $4M_A$ domain structures featuring a 180°/71° domain wall type and a 180°/109° domain wall type. A Type 3 domain structure has a pure 109° domain wall type. Detailed electrical switching properties have been studied through the SSPFM mappings, and the divergence of coercive fields in different types of domains is likely to be associated with different domain sizes and types. Furthermore, the perfect correlation between the morphology and ferroelectric domains allows for pinpointing diverse domain structures using optical microscopy. The detailed study of PMN-30PT single crystal at mesoscale can provide a better understanding of various domain structures and insight into the structure-property relationship of the material.

DECLARATIONS

Authors' contributions

Experimental design: Zhang D, Seidel J
Experiments and data collection: Zhang D, Wang L
Data analysis: Zhang D, Wang L, Li L, Sharma P
Manuscript writing and revision: Zhang D, Wang L, Li L, Sharma P, Seidel J
Supervision: Seidel J

Availability of data and materials

The data that support the findings of this study are available from the corresponding author upon reasonable request.

Financial support and sponsorship

This work was supported by the Australian Research Council through Discovery Grants and the ARC Centre of Excellence in Future Low Energy Electronics Technologies (FLEET), the National Natural Science Foundation of China (No. 12204096), the Natural Science Foundation of Jiangsu Province (BK20220797), the Open Research Fund Program of the State Key Laboratory of Low-Dimensional Quantum Physics (No. KF202203), the open research fund of Key Laboratory of Quantum Materials and Devices (Southeast University), Ministry of Education, the Fundamental Research Funds for the Central Universities, an Australian Government Research Training Program (RTP) Scholarship, the Flinders University start-up grant. Some of the data presented in this work was acquired using instruments at the Mark Wainwright Analytical Centre (MWAC) of UNSW Sydney with the assistance of personnel, which is in part funded by the Research Infrastructure Programme of UNSW.

Conflicts of interest

All authors declared that there are no conflicts of interest.

Ethical approval and consent to participate

Not applicable.

Consent for publication

Not applicable.

REFERENCES

1. Park SE, Shrout TR. Ultrahigh strain and piezoelectric behavior in relaxor based ferroelectric single crystals. *J Appl Phys* 1997;82:1804-11. DOI
2. Fu H, Cohen RE. Polarization rotation mechanism for ultrahigh electromechanical response in single-crystal piezoelectrics. *Nature* 2000;403:281-3. DOI PubMed
3. Qiu C, Wang B, Zhang N, et al. Transparent ferroelectric crystals with ultrahigh piezoelectricity. *Nature* 2020;577:350-4. DOI
4. Li F, Cabral MJ, Xu B, et al. Giant piezoelectricity of Sm-doped $Pb(Mg_{1/3}Nb_{2/3})O_3$-$PbTiO_3$ single crystals. *Science* 2019;364:264-8. DOI
5. Li F, Lin D, Chen Z, et al. Ultrahigh piezoelectricity in ferroelectric ceramics by design. *Nat Mater* 2018;17:349-54. DOI
6. Li L, Yang Y, Zhang D, et al. Machine learning-enabled identification of material phase transitions based on experimental data: exploring collective dynamics in ferroelectric relaxors. *Sci Adv* 2018;4:eaap8672. DOI PubMed PMC
7. Zhang S, Shrout TR. Relaxor-PT single crystals: observations and developments. *IEEE Trans Ultrason Ferroelectr Freq Control* 2010;57:2138-46. DOI PubMed PMC
8. Singh AK, Pandey D. Evidence for M_B and M_C phases in the morphotropic phase boundary region of(1-x)[$Pb(Mg_{1/3}Nb_{2/3})O_3$]-x$PbTiO_3$: a rietveld study. *Phys Rev B* 2003;67:064102. DOI

9. Sun E, Cao W. Relaxor-based ferroelectric single crystals: growth, domain engineering, characterization and applications. *Prog Mater Sci* 2014;65:124-210. DOI PubMed PMC
10. Wada S, Yako K, Kakemoto H, Tsurumi T, Kiguchi T. Enhanced piezoelectric properties of barium titanate single crystals with different engineered-domain sizes. *J Appl Phys* 2005;98:014109. DOI
11. Wada S, Suzuki S, Noma T, et al. Enhanced piezoelectric property of barium titanate single crystals with engineered domain configurations. *Jpn J Appl Phys* 1999;38:5505. DOI
12. Vanderbilt D, Cohen MH. Monoclinic and triclinic phases in higher-order Devonshire theory. *Phys Rev B* 2001;63:094108. DOI
13. Park MH, Lee YH, Kim HJ, et al. Morphotropic phase boundary of $Hf_{1-x}Zr_xO_2$ thin films for dynamic random access memories. *ACS Appl Mater Interfaces* 2018;10:42666-73. DOI
14. Sarott MF, Rossell MD, Fiebig M, Trassin M. Multilevel polarization switching in ferroelectric thin films. *Nat Commun* 2022;13:3159. DOI PubMed PMC
15. Chang WY, Chung CC, Yuan ZY, et al. Patterned nano-domains in PMN-PT single crystals. *Acta Mater* 2018;143:166-73. DOI
16. Yamamoto Y, Itsumi K, Hosono Y. Effects of manganese oxides/gold composite electrode on piezoelectric properties of lead magnesium niobate titanate single crystal. *Jpn J Appl Phys* 2011;50:09NC05. DOI
17. Luo C, Wan H, Chang WY, et al. Effect of low-frequency alternating current poling on 5-mm-thick $0.7Pb(Mg_{1/3}Nb_{2/3})O_3$-$0.3PbTiO_3$ single crystals. *Appl Phys Lett* 2019;115:192904. DOI
18. Wan H, Luo C, Chang WY, Yamashita Y, Jiang X. Effect of poling temperature on piezoelectric and dielectric properties of $0.7Pb(Mg_{1/3}Nb_{2/3})O_3$-$0.3PbTiO_3$ single crystals under alternating current poling. *Appl Phys Lett* 2019;114:172901. DOI
19. Yamashita Y, Yamamoto N, Hosono Y, Itsumi K. Piezoelectric transducer, ultrasonic probe, and piezoelectric transducer manufacturing method. 2015. Available from: https://patents.google.com/patent/US20150372219 [Last accessed on 1 Dec 2023].
20. Yamamoto N, Yamashita Y, Hosono Y, Itsumi K, Higuchi K. Ultrasonic probe, piezoelectric transducer, method of manufacturing ultrasonic probe, and method of manufacturing piezoelectric transducer. 2014. Available from: https://patents.google.com/patent/US20140062261A1/en [Last accessed on 1 Dec 2023]
21. Deng C, Ye L, He C, et al. Reporting excellent transverse piezoelectric and electro-optic effects in transparent rhombohedral PMN-PT single crystal by engineered domains. *Adv Mater* 2021;33:e2103013. DOI
22. Chang WY, Chung CC, Luo C, et al. Dielectric and piezoelectric properties of 0.7 $Pb(Mg_{1/3}Nb_{2/3})O_3$-0.3 $PbTiO_3$ single crystal poled using alternating current. *Mater Res Lett* 2018;6:537-44. DOI
23. Wan H, Luo C, Liu C, Chang WY, Yamashita Y, Jiang X. Alternating current poling on sliver-mode rhombohedral $Pb(Mg_{1/3}Nb_{2/3})O_3$-$PbTiO_3$ single crystals. *Acta Mater* 2021;208:116759. DOI
24. Xu J, Deng H, Zeng Z, et al. Piezoelectric performance enhancement of $Pb(Mg_{1/3}Nb_{2/3})O_3$-$0.25PbTiO_3$ crystals by alternating current polarization for ultrasonic transducer. *Appl Phys Lett* 2018;112:182901. DOI
25. Zhuo F, Zhou X, Gao S, et al. Anisotropic dislocation-domain wall interactions in ferroelectrics. *Nat Commun* 2022;13:6676. DOI PubMed PMC
26. Zhuo F, Zhou X, Gao S, et al. Intrinsic-strain engineering by dislocation imprint in bulk ferroelectrics. *Phys Rev Lett* 2023;131:016801. DOI
27. Zhang D, Sando D, Pan Y, Sharma P, Seidel J. Robust ferroelectric polarization retention in harsh environments through engineered domain wall pinning. *J Appl Phys* 2021;129:014102. DOI
28. Zhang D, Sando D, Sharma P, et al. Superior polarization retention through engineered domain wall pinning. *Nat Commun* 2020;11:349. DOI PubMed PMC
29. Bai F, Li J, Viehland D. Domain hierarchy in annealed (001)-oriented $Pb(Mg_{1/3}Nb_{2/3})O_3$-x%$PbTiO_3$ single crystals. *Appl Phys Lett* 2004;85:2313-5. DOI
30. Rodriguez BJ, Jesse S, Morozovska AN, et al. Real space mapping of polarization dynamics and hysteresis loop formation in relaxor-ferroelectric $PbMg_{1/3}Nb_{2/3}O_3$-$PbTiO_3$ solid solutions. *J Appl Phys* 2010;108:042006. DOI
31. Bian JH, Xue P, Zhu R, et al. Fingerprints of relaxor ferroelectrics: characteristic hierarchical domain configurations and quantitative performances. *Appl Mater Today* 2020;21:100789. DOI
32. Luo CT, Chang WY, Gao M, et al. Multi-layered domain morphology in relaxor single crystals with nano-patterned composite electrode. *Acta Mater* 2020;182:10-7. DOI
33. Finkel P, Cain MG, Mion T, et al. Simultaneous large optical and piezoelectric effects induced by domain reconfiguration related to ferroelectric phase transitions. *Adv Mater* 2022;34:e2106827. DOI
34. Liu HJ, Chen HJ, Liang WI, et al. Structural study in highly compressed $BiFeO_3$ epitaxial thin films on $YAlO_3$. *J Appl Phys* 2012;112:052002. DOI
35. Christen HM, Nam JH, Kim HS, Hatt AJ, Spaldin NA. Stress-induced *R-MA-MC-T* symmetry changes in $BiFeO_3$ films. *Phys Rev B* 2011;83:144107. DOI
36. Chen C, Chen D, Li P, et al. Deterministic manipulation of multi-state polarization switching in multiferroic thin films. *Adv Funct Mater* 2023;33:2208244. DOI
37. Sharma P, Zhang Q, Sando D, et al. Nonvolatile ferroelectric domain wall memory. *Sci Adv* 2017;3:e1700512. DOI PubMed PMC
38. Li L, Xie L, Pan X. Real-time studies of ferroelectric domain switching: a review. *Rep Prog Phys* 2019;82:126502. DOI
39. Khakpash N, Khassaf H, Rossetti GA, Alpay SP. Misfit strain phase diagrams of epitaxial PMN-PT films. *Appl Phys Lett* 2015;106:082905. DOI

40. Belhadi J, Gabor U, Ursic H, et al. Growth mode and strain effect on relaxor ferroelectric domains in epitaxial $0.67Pb(Mg_{1/3}Nb_{2/3})O_3$-$0.33PbTiO_3$/$SrRuO_3$ heterostructures. *RSC Adv* 2021;11:1222-32. DOI PubMed PMC